HHS Public Access

Author manuscript

Sci Transl Med. Author manuscript; available in PMC 2024 August 20.

Published in final edited form as:

Sci Transl Med. 2024 May 22; 16(748): eadj4504. doi:10.1126/scitranslmed.adj4504.

The oral nucleoside prodrug GS-5245 is efficacious against SARS-CoV-2 and other endemic, epidemic and enzootic coronaviruses

David R. Martinez[1,2,*], **Fernando R. Moreira**[3], **Nicholas J. Catanzaro**[3], **Meghan V. Diefenbacher**[3], **Mark R. Zweigart**[3], **Kendra L. Gully**[3], **Gabriela De la Cruz**[4], **Ariane J. Brown**[3], **Lily E. Adams**[3], **Boyd Yount**[3], **Thomas J. Baric**[3], **Michael L. Mallory**[3], **Helen Conrad**[3], **Samantha R. May**[3], **Stephanie Dong**[3], **D. Trevor Scobey**[3], **Cameron Nguyen**[3], **Stephanie A. Montgomery**[5], **Jason Perry**[6], **Darius Babusis**[6], **Kimberly T. Barrett**[6], **Anh-Hoa Nguyen**[6], **Anh-Quan Nguyen**[6], **Rao Kalla**[6], **Roy Bannister**[6], **Joy Y. Feng**[6], **Tomas Cihlar**[6], **Ralph S. Baric**[3,7,8], **Richard L. Mackman**[6,&], **John P. Bilello**[6,*], **Alexandra Schäfer**[3,8,*], **Timothy P. Sheahan**[3,7,8,*]

[1]Department of Immunobiology, Yale School of Medicine, New Haven, CT, 06510, USA

[2]Yale Center for Infection and Immunity, Yale School of Medicine, New Haven, CT, 06510, USA

[3]Department of Epidemiology, University of North Carolina at Chapel Hill, Chapel Hill, NC, 27599, USA

[4]Lineberger Comprehensive Cancer Center, University of North Carolina School of Medicine, Chapel Hill, NC, 27599, USA

[5]Department of Pathology and Laboratory Medicine, University of North Carolina School of Medicine, Chapel Hill, NC, 27599, USA

[6]Gilead Sciences, Inc, Foster City, CA, 94404, USA

[7]Department of Microbiology and Immunology, University of North Carolina School of Medicine, Chapel Hill, NC, 27599, USA

[8]Rapidly Emerging Antiviral Drug Development Initiative, University of North Carolina at Chapel Hill, Chapel Hill, NC, 27599, USA

[*]Correspondence: david.martinez@yale.edu (D.R.M.), john.bilello@gilead.com (J.P.B.), aschaefer@email.unc.edu (A.S.), sheahan@email.unc.edu (T.P.S.).

[&]Current Address: 360 Ashton Ave, Millbrae, CA94030 mackmanmedchem@gmail.com

AUTHOR CONTRIBUTIONS

The studies were conceived and designed by D.R.M., N.J.C., A.S., T.P.S., J.P., D.B., R.B., J.Y.F., T.C., R.S.B., R.L.M., and J.P.B.. The studies were performed by D.R.M., F.R.M., N.J.C., M.V.D., M.R.Z., K.L.G., G.D.l.C., A.J.B., L.E.A., B.Y., T.J.B., M.L.M., H.C., S.R.M., S.D., D.T.S., S.A.M., J.P., D.B., K.T.B., A-Q.N., R.K., R.L.M, A.S. and T.P.S. Data was analyzed by D.R.M., F.R.M., N.J.C., M.V.D., C.N., S.A.M., J.P., D.B., A-H.N., J.Y.F., R.L.M., J.P.B., A.S. and T.P.S.. Critical reagents were supplied by K.T.B., A-Q.N., R.K., R.B, J.P.B., J.Y.F., T.C., and R.L.M.. Figures were generated by D.R.M., F.R.M., N.J.C., M.V.D., L.E.A., S.A.M., J.P., A.S. and T.P.S. The manuscript was written and edited by D.R.M., N.J.C., J.P., D.B., J.Y.F., T.C., R.S.B., R.L.M., J.P.B., A.S. and T.P.S. All authors reviewed and approved the manuscript.

COMPETING INTERESTS

Gilead patents related to this work are: Methods and compounds for treating paramyxoviridae virus infections WO2012/012776, Methods for treating arenaviridae and coronaviridae virus infections WO2017/049060 and Methods for treating SARS-CoV-2 infections WO/2021/154687. These authors current or former employees of Gilead Sciences and hold stock in Gilead Sciences: D.B., A.N., K.T.B., R.B, J.P.B., J.Y.F., T.C., and R.L.M. R.S.B. is a member of advisory boards for VaxArt, Takeda and Invivyd, and has collaborative unrelated projects with J&J, and Hillevax. All other authors declare no competing interests.

Abstract

Despite the wide availability of several safe and effective vaccines that prevent severe COVID-19, the persistent emergence of SARS-CoV-2 variants of concern (VOCs) that can evade vaccine-elicited immunity remains a global health concern. In addition, the emergence of SARS-CoV-2 VOCs that can evade therapeutic monoclonal antibodies underscores the need for additional, variant-resistant treatment strategies. Here, we characterize the antiviral activity of GS-5245, obeldesivir (ODV), an oral prodrug of the parent nucleoside GS-441524, which targets the highly conserved RNA-dependent viral RNA polymerase (RdRp). We show that GS-5245 is broadly potent in vitro against alphacoronavirus HCoV-NL63, severe acute respiratory syndrome coronavirus (SARS-CoV), SARS-CoV-related bat-CoV RsSHC014, Middle East Respiratory Syndrome coronavirus (MERS-CoV), SARS-CoV-2 WA/1, and the highly transmissible SARS-CoV-2 BA.1 Omicron variant. Moreover, in mouse models of SARS-CoV, SARS-CoV-2 (WA/1 and Omicron B1.1.529), MERS-CoV, and bat-CoV RsSHC014 pathogenesis, we observed a dose-dependent reduction in viral replication, body weight loss, acute lung injury, and pulmonary function with GS-5245 therapy. Finally, we demonstrate a combination of GS-5245 and main protease (M^{pro}) inhibitor nirmatrelvir improved outcomes in vivo against SARS-CoV-2 compared to the single agents. Altogether, our data supports the clinical evaluation of GS-5245 against coronaviruses which cause or have the potential to cause human disease.

One sentence summary:

The small molecule GS-5245 is therapeutically efficacious in animals infected with different pandemic, epidemic or enzootic coronaviruses.

Editor’s Summary:

A Versatile Antiviral. Currently-approved antivirals for SARS-CoV-2 target one of two viral proteins. Remdesivir and molnupiravir target the RNA-dependent RNA polymerase (RdRp), whereas nirmaltrelvir (the antiviral agent of Paxlovid) targets the main protease (M^{pro}). Although these drugs are effective, there continues to be room for improvement, especially for drugs targeting the RdRp. Here, Martinez *et al.* evaluated the efficacy of an orally available small molecule targeting the RdRp of SARS-CoV-2 and other coronaviruses called GS-5245 or obeldesivir. The authors found that GS-5245 could reduce disease severity in mice infected with one of several different coronaviruses, including SARS-CoV-2, SARS-CoV, and MERS-CoV. Moreover, combining GS-5245 with nirmatrelvir further improved outcomes in mice infected with SARS-CoV-2. Together, these data support further development of GS-5235/Obeldesivir as a broader anti-coronaviral drug. –Courtney Malo

INTRODUCTION

The emergence of three highly pathogenic novel coronaviruses (CoVs) into immunologically naïve human populations in the last two decades underlines an urgent need to develop broad-acting countermeasures. Although broad-spectrum vaccines (1-3) and monoclonal antibodies (4-7) have shown promise in animal models against the sarbecovirus subgenus, the spike protein has extensively mutated throughout the coronavirus disease 2019 (COVID-19) pandemic, resulting in variants of concern (VOCs) that have partially or

fully evaded vaccines and clinically used monoclonal antibody therapies (8). In contrast, highly conserved viral enzymes, like the RNA-dependent RNA polymerase (RdRp, non-structural protein 12, nsp12) or main protease (M^{pro}, nsp5) are more genetically stable and thus represent optimal targets for broad-spectrum antivirals. As broadly acting antivirals targeting the CoV RdRp, both Veklury (remdesivir, RDV) and Lagevrio (molnupiravir, MOV) have antiviral activity in vitro and in vivo against SARS-CoV-2 and divergent coronaviruses (9-16) and have been deployed for human use in the COVID-19 pandemic (17, 18). The M^{pro} inhibitor nirmatrelvir (PF-07321332), the active antiviral agent in Paxlovid (nirmatrelvir/ritonavir, PAX), exerts strong antiviral activity in vitro and in SARS-CoV-2 animal models (19). Importantly remdesivir, molnupiravir and Paxlovid all improve outcomes in patients with COVID-19 when given early in the course of infection (18, 20-22) and thus far have retained their antiviral activity against SARS-CoV-2 VOCs including Omicron (16, 23). However, with the continued emergence of SARS-CoV-2 variants and increased use of antiviral monotherapy, it is critical to strengthen our armamentarium of orally bioavailable drugs and their combinations to treat COVID-19 in all populations, reduce its impact on the health care system, and minimize the development of antiviral resistance.

Here, we tested the antiviral efficacy of GS-5245 (obeldesivir, ODV) an oral prodrug of the nucleoside analog, GS-441524 (24). GS-5245 has increased cellular permeability over GS-441524 and is rapidly cleaved pre-systemically in the gastrointestinal system to deliver GS-441524 into systemic circulation at higher exposures than what is achieved through direct oral dosing at an equivalent molar dose of GS-441524 in non-human primates (24-27). In effect, the prodrug affords higher oral bioavailability of GS-441524 in non-human primates, thereby reducing the amount of GS-441524 that is eliminated during the oral absorption process. We show that GS-5245 has broad antiviral activity in vitro against endemic, enzootic, and pandemic coronaviruses including NL63, bat SARS-related RsSHC014-CoV, SARS-CoV, MERS-CoV, the ancestral SARS-CoV-2 WA1, and the highly transmissible SARS-CoV-2 Omicron BA.1 variant. Importantly, oral GS-5245 therapy diminished replication and disease against SARS-CoV, RsSHC014-CoV, SARS-CoV-2 WA/1, SARS-CoV-2 Omicron BA.1 and MERS-CoV; a demonstration of its efficacy and breadth in vivo. Moreover, a combination GS-5245 and nirmatrelvir improved therapeutic efficacy against SARS-CoV-2 in mice compared to each single agent. These results support the exploration of GS-5245 in human clinical trials and exemplify a potential benefit of COVID-19 antiviral combination therapy.

RESULTS

GS-5245 is broadly active against a panel of enzootic, endemic, and pandemic coronaviruses in primary human airway cells

We first evaluated the antiviral activity of the GS-5245, its parent nucleoside GS-441524, remdesivir, and the M^{pro} inhibitor nirmatrelvir, against a SARS-CoV-2 WA/1 nanoluciferase reporter virus in A549 cells that overexpress human ACE2 (Fig. 1A, fig. S1). GS-5245 potently inhibited SARS-CoV-2 replication (half-maximal effective concentration (EC_{50}) 0.74 μM) without cytotoxicity (Fig. 1A and fig. S2). Consistent with prior reports,

remdesivir, GS-441524 and nirmatrelvir strongly inhibited SARS-CoV-2 replication with EC_{50} values of 0.19, 4.6, and 0.07 μM respectively (Fig. 1A and fig. S2) (11, 19). The improved activity of GS-5245 over parent nucleoside GS-441524 in these cells was likely due to improved cellular permeability, including unexpectedly favorable interactions with nucleoside transporters that resulted in elevated concentrations of the active nucleoside triphosphate species that inhibits the viral RNA-dependent RNA polymerase (24). To assess the antiviral breadth of GS-5245 against alphacoronavirus, we designed a reverse genetic system for endemic common cold causing coronavirus HCoV-NL63. Recombinant nanoluciferase (nLUC) expressing NL63 (NL63-nLUC) (fig. S3A) replicated similarly to wild-type virus (fig. S3B) and highly expressed reporter nanoluciferase (fig. S3C). GS-5245, remdesivir and GS-441524 similarly exerted robust antiviral activity against NL63-nLUC without cytotoxicity in LLC-MK2-TMPRSS2 cells with respective EC_{50} values of 0.62, 0.50, and 0.52 μM, respectively (fig. S4A to C).

To further evaluate the breadth of GS-5245 antiviral activity against enzootic, endemic, epidemic, and pandemic coronaviruses, including highly transmissible SARS-CoV-2 variants, we evaluated GS-5245 in primary human airway epithelial (HAE) cells from two different human donors. The HAE platform is a biologically relevant three-dimensional culture system which models the structure and cellular complexity of the conducting airway and importantly contains epithelial target cells of CoVs (28). Although a donor-dependent variation in infection efficiency was evident with some of the viruses we utilized, a GS-5245 dose-dependent reduction in infectious virus production was observed for all viruses tested including SARS-CoV Urbani, bat-CoV RsSHC014, SARS-CoV-2 WA/1, the highly transmissible Omicron BA.1 variant, and MERS-CoV in HAE without measurable cytotoxicity across the dose range assessed (Fig. 1B and C, fig. S5). These studies demonstrate the antiviral potency of the prodrug GS-5245 following metabolism to the active nucleoside triphosphate, which occurs in HAE cell cultures susceptible to our panel of CoVs. In conclusion, GS-5245 has potent activity against a broad array of genetically distinct CoVs in cell lines and biologically relevant primary cell systems.

The broad activity exhibited by GS-5245 is likely driven by structural conservation in the RdRp across the CoV family. The residues in the nsp12 RdRp polymerase F-motif (V557 and A558) and B-motif (T687) that help position the template in the active site and guide nucleotide incorporation are highly conserved (29). These residues also guide the antiviral activity of GS-443902 (fig. S1), the active nucleoside triphosphate metabolite of GS-5245, GS-441524, and RDV. T687 is a key residue in the recognition of the inhibitor, which is more efficiently incorporated during RNA synthesis than native ATP whereas V557 and A558 play a role in template-dependent inhibition, one of the antiviral mechanisms of action for GS-443902 (26, 30). Although the RdRp protein surface amino acid residue conservation was as low as 59% in HcoV-NL63 compared to SARS-CoV-2, the residues noted above that could impact GS-443902 potency were 100% conserved across these and several other human and enzoonotic coronaviruses (fig. S6), demonstrating the potential for pancoronavirus antiviral activity of nucleoside analogs targeting these residues of the SARS-CoV-2 RdRp.

GS-5245 exhibits therapeutic efficacy against mouse-adapted SARS-CoV-2 challenge in BALB/c mice

First, we evaluated the pharmacokinetics of GS-5245 in the three mouse strains utilized in our studies (fig. S7). Since GS-5245 is extensively metabolized pre-systemically in the digestive system to deliver GS-441524 to the systemic circulation, we measured GS-441524 in BALB/c (Sarbecovirus models), C57BL/6 where residues 288 and 330 of mouse dipeptidyl peptidase 4 were modified to the orthologous human residues (288/330 mDPP4, MERS-CoV transgenic model), and C57BL/6 K18-hACE2 (Sarbecovirus models) plasma over 24hr following oral administration (fig. S7A). The daily systemic exposure of GS-441524 following twice daily (bis in die; BID) oral dosing at 30 mg/kg of GS-5245 across the different mouse strains was anticipated to range from 81 to 108 μM·h. No intact GS-5245 prodrug was observed at any timepoint sampled (fig. S7B). This exposure of GS-441524 is consistent with those achieved following oral administration of a tri-ester prodrug of GS-441524, GS-621763, dosed at 30 mg/kg BID in our earlier efficacy studies (24, 31).

To determine the optimal therapeutic dose of GS-5245 in mice, we performed a therapeutic dose-ranging study in SARS-CoV-2 MA10-infected ($1x10^4$ plaque forming units; PFU) BALB/c mice. We initiated therapy 12 hr post infection (hpi) with vehicle or 3, 10, or 30 mg/kg GS-5245 diluted in vehicle and mice were dosed orally BID through 4 days post infection (dpi). We also included a cohort treated orally with molnupiravir (MOV) at 100 mg/kg BID, a human equivalent dose determined based on the area under the curve (AUC) exposure. Overall, there was a distinct GS-5245 dose-dependent reduction in virus replication and pathogenesis (Fig. 2A to F). Mice treated with 3 mg/kg GS-5245 had measurable weight loss similar to vehicle, macroscopic lung discoloration, viral-induced pulmonary dysfunction and measures of acute lung injury (ALI) as measured by two scoring systems (e.g. ATS and DAD) we have optimized previously for multiple emerging CoV (Fig. 2A to F) (11, 12, 32). The ATS scoring system broadly reports histologic manifestations of ALI (e.g. neutrophils in alveolar septae or in airspaces, hyaline membranes, proteinaceous debris in airway, alveolar septal thickening), whereas the DAD score more specifically reports phenotypes of diffuse alveolar damage (e.g. cellular sloughing, necrosis, hyaline membranes), the pathological hallmarks of ALI. Protection from weight loss, lung titer and gross lung pathology (lung discoloration) (Fig. 2A to C) was conferred by a higher dose of GS-5245 (10 mg/kg), although this protective effect was not extended to improved pulmonary function or lung pathology (Fig. 2D to F). Mice receiving the highest dose of GS-5245 (30 mg/kg) or MOV (100 mg/kg) were protected against developing all metrics of disease including body weight loss (Fig. 2A), virus replication (Fig. 2B), gross lung pathology (Fig. 2C), loss of pulmonary function (Fig. 2D) and acute lung injury (Figs. 2E and F) observed in the vehicle arm.

Prior studies with remdesivir indicated that therapy concurrent with or after the peak of virus replication (24 to 48hr) afforded some protection from virus replication but not from SARS-CoV-2 disease (14, 32). To determine the time at which a robust dose of GS-5245 therapy (30mg/kg) fails to improve outcomes in mice, we performed a therapeutic efficacy study initiating treatment in SARS-CoV-2 MA10 infected ($1x10^4$ PFU) BALB/c mice at

12, 24, and 36 hpi (fig. S8). GS-5245 therapy initiated at 12 or 24 hpi protected from body weight loss, lung viral replication, gross lung pathology, and degradation of pulmonary function (fig. S8A to F) whereas therapy initiated at 36 hpi reduced virus replication but had little impact on disease. Similar observations were made in studies using a lower dose of GS-5245 (10 mg/kg) administered at 12, 24, and 36 hpi (fig. S9A to F), although therapy initiated with the lower dose of GS-5245 at 24hr after infection offered less robust protection than that of 30 mg/kg. Altogether, these data demonstrate a strong dose- and time-dependent relationship between protection from SARS-CoV-2 disease and GS-5245 therapy. Therapy was most successful if initiated prior to the peak of virus replication.

GS-5245 is effective against SARS-related bat-CoV RsSHC014 in K18-hACE mice

We next aimed to understand the breadth of in vivo therapeutic efficacy against more distantly related Sarbecoviruses. We performed a therapeutic efficacy study in C57BL/6 K18-hACE2 mice with the SARS-like bat-CoV RsSHC014, a bat virus previously shown to efficiently replicate in HAE cell cultures and to evade SARS-CoV-2 vaccines and monoclonal antibodies developed for the original SARS-CoV (3, 33). We initiated GS-5245 therapy at 12 or 24 hpi, which demonstrated success in SARS-CoV-2 models above. Unlike the SARS-CoV-2 MA10 BALB/c model, weight loss is not typically associated with RsSHC014 infection, although we did observe increased weight in the infected animals dosed with 30 mg/kg GS-5245 initiated at 12 hpi compared to vehicle-treated mice (Fig. 3A). Whereas animals treated with 10mg/kg GS-5245 did not exhibit reduced viral titers (Fig. 3B) and gross lung pathology (Fig. 3C), those treated with the higher 30 mg/kg dose had reduced virus lung titers and gross lung pathology compared with controls, irrespective of initiation time. Using histologic tools described above for the SARS-CoV-2 MA10 model, we determined that groups receiving 30 mg/kg initiated at 12 hpi had reduced acute lung injury scores with both scoring tools (Fig. 3D and E) whereas therapy initiated 24 hpi facilitated reductions in DAD scores only (Fig. 3E). Thus, GS-5245 therapy reduced the replication and disease caused by the SARS-related bat virus, RsSHC014 in C57BL/6 K18-hACE2 mice.

GS-5245 protects against SARS-CoV MA15 mortality in BALB/c mice

In November 2002, SARS-CoV emerged in the Guangdong Province of China, ultimately causing over 8000 cases in 29 countries and over 800 deaths with a 10% mortality rate (34, 35). Although this global epidemic was ultimately contained and eradicated by public health measures, viruses similar to the SARS-CoV epidemic strain have been found in classic reservoir species in China and remain a public health threat (33, 36). Thus, we next evaluated the therapeutic efficacy of GS-5245 against SARS-CoV in BALB/c mice using the highly pathogenic mouse-adapted SARS-CoV MA15 virus in studies similar in design to those described in Fig. 3(37). Unlike the above SARS-CoV-2 studies, only 30 mg/kg GS-5245 initiated at 12 hpi protected animals from body weight loss observed in vehicle controls (Fig. 4A) and reduced viral replication (Fig. 4B) and gross lung pathology (Fig. 4C). SARS-CoV MA15 infection causes mortality in BALB/c mice (37). We observed a time- and dose-dependent effect on survival, with 100% and 70% survival in the 30- and 10-mg/kg GS-5245 groups at 12 hpi, respectively (Fig. 4D). Delay of treatment initiation with either dose of GS-5245 resulted in mortality comparable to the vehicle control group.

Congruent with the body weight loss data, only 30 mg/kg initiated at 12 hpi protected from the development of acute lung injury as determined by DAD but not ATS scoring schema (Fig. 4E and F) indicating that the differences in lung pathology at this time were best described by the DAD score which more specifically reports direct damage to the lung epithelium. Congruent with body weight loss data, 30 mg/kg initiated at 12 hpi prevented the loss of pulmonary function observed in the vehicle on days 1 and 2 (Fig. 4G). Thus, early treatment with a 30 mg/kg dose of GS-5245 was protective against SARS-CoV disease symptoms and mortality in mice.

GS-5245 therapy protects against MERS-CoV pathogenesis in mice

MERS-CoV is endemic in camels in the Middle East and Northeast Africa and frequently spills over into humans, causing severe respiratory virus infection (38-40). Using a mouse model where murine DPP4 has been humanized at residues 288 and 330 to facilitate infection, we performed a therapeutic efficacy study to determine if 10 or 30 mg/kg GS-5245 would diminish replication and improve pathogenic outcomes at 12 hpi given that therapy initiated at this time post infection was most successful in the SARS-CoV model above(41, 42). In agreement with the SARS-CoV-2 and SARS-CoV in vivo data above, GS-5245 at 30 mg/kg provided the best protection against signs of clinical disease including weight loss, lung viral titers, acute lung injury, and degradation in respiratory function (Fig. 5A to F). Whereas the lower 10 mg/kg dose only afforded partial protection from weight loss (Fig. 5A), it reduced lung viral replication (Fig. 5B). However, the lower dose again failed to improve gross lung pathology (Fig. 5C), pulmonary function (Fig. 5D), or histologic metrics of acute lung injury (Fig. 5E and F). Thus, early GS-5245 therapy at 30mg/kg protected against MERS-CoV pathogenesis in mice.

GS-5245 therapy potently reduces SARS-CoV-2 Omicron replication in K18-hACE2 mice

As we observed a high degree of protection against bat RsSHC014-CoV, SARS-CoV, MERS-CoV, and a mouse-adapted SARS-CoV-2 based on the Wuhan-1 isolate, we sought to evaluate GS-5245 against the highly transmissible Omicron (B.1.1.529/BA.1) variant in K18-hACE2 mice. Consistent with Halfman *et al.*, we did not observe body weight loss following Omicron infection during our 4-day study (Fig. 6A) (43). Mice treated with GS-5245 at 30 mg/kg 12 hpi had lower lung viral titers relative to vehicle-treated groups at 2 and 3 dpi (Fig. 6B), and less macroscopic lung pathology (Fig. 6C). Unlike ATS ALI scores (Fig. 6D), DAD scores were different among vehicle and treated animals (Fig. 6E). From these data, we conclude that GS-5245 therapy is effective at reducing Omicron BA.1 replication in mice.

Combination therapy of nirmatrelvir and GS-5245 protects against SARS-CoV-2 in BALB/c mice

As the oral antiviral nirmatrelvir (PF-07321332) demonstrated a high degree of efficacy in mice and humans (19, 20), we sought to evaluate if combination of nirmatrelvir with GS-5245 at suboptimal doses would improve outcomes over single agent therapy in mice. Nirmatrelvir inhibits M^{pro} by preventing processing of the viral polyprotein whereas GS-5245 inhibits the RdRp by terminating transcription and replication (25) or by excessive polymerase pausing (44). We first performed a dose-descending study to determine the

optimal and suboptimal doses of nirmatrelvir in our SARS-CoV-2 model (fig. S10). As expected, nirmatrelvir therapy twice daily exhibited a dose-dependent protective effect on body weight loss, viral replication, gross lung pathology and pulmonary function (fig. S10A to D). Very low doses of GS-5245 (1.2 mg/kg) and nirmatrelvir (12 mg/kg) did little to diminish weight loss, viral replication and gross lung pathology, yet had a moderate effect on improving pulmonary function (fig. S10A to D). We then performed a dose range-finding combination therapy study to identify conditions where combination therapy improved outcomes over suboptimal doses of single agents. We focused first on evaluating viral lung titers, since prevention of replication with early therapy was associated with diminished pathogenesis in prior studies. Mice infected with SARS-CoV-2 were treated twice daily with suboptimal doses of single agents (GS-5245 at 1.2 or 4 mg/kg, nirmatrelvir at 12 or 40 mg/kg) or several combinations including: “low dose combination” of 1.2 mg/kg GS-5245 + 12 mg/kg nirmatrelvir, “medium dose combination” of 1.2 mg/kg GS-5245 + 40 mg/kg nirmatrelvir, or “high dose combination” of 4 mg/kg GS-5245 + 40 mg/kg nirmatrelvir. As compared with vehicle-treated animals, we observed drug dose-dependent reductions in the viral lung titers with both single agents and combination therapies (fig. S10E). Importantly, the high dose combination (4 mg/kg GS-5245 + 40 mg/kg nirmatrelvir) reduced viral lung titers more than either single agent (4mg/kg GS-5245 or 40mg/kg nirmatrelvir) (fig. S10E).

Building off of the dose finding studies above, we then performed a second focused study to determine the effect of therapy with suboptimal single agents (4 mg/kg GS-5245 or 40 mg/kg nirmatrelvir) or combination therapy (4 mg/kg GS-5245 + 40 mg/kg nirmatrelvir) on weight loss, viral replication on 2 and 4 dpi, gross and microscopic lung pathology, pulmonary function, and the lung transcriptome in mice infected with SARS-CoV-2. Suboptimal single agent and combination therapy similarly provided protection from body weight loss (Fig. 7A) yet only single agents afforded protection from loss of pulmonary function on 3 dpi (Fig. 7B). On 2 dpi, single agent and combination therapy reduced viral lung titers (Fig. 7C) as compared to vehicle treated animals. On 4 dpi, the benefits of combination therapy were readily apparent, with greater titer reductions than each individual single agent (Fig. 7D). This reduction in infectious titers was supported by staining of lung tissue sections for viral antigen (fig. S11 and 12). Similarly, combination therapy provided protection from lung discoloration, a macroscopic measure of lung pathology, as compared with vehicle-treated animals and animals treated with nirmatrelvir alone (Fig. 7E). We then analyzed lung tissue sections for pathology and scored histologic metrics of ALI (fig. S13). Similar to prior studies with SARS-CoV-2 MA10 (45, 46), in vehicle-treated animals, we found scattered areas of degenerating and dying cells with a moderate multifocal immune infiltrate comprised of lymphocytes and neutrophils predominantly in the alveolar interstitium and less frequently in the alveolar airspace (fig. S13). Scattered airspaces contained proteinaceous debris from capillary leakage. These histologic phenotypes noted in vehicle-treated animals were less apparent with suboptimal monotherapy and with combination therapy (fig. S13). Upon quantitating the histologic manifestations of acute lung injury, combination therapy was the only group with improved ATS acute lung injury scores (Fig. 7F). Using a complementary histologic scoring tool that specifically assesses features of diffuse alveolar damage, we found that all treatment groups were similarly protected against DAD (Fig. 7G).

To investigate the effect of sub-optimal monotherapy or combination therapy on the host response, we performed bulk RNA-sequencing on total lung RNA from an uninfected cohort of animals along with samples from animals described in Fig. 7. Like the virologic data above, viral RNA was reduced by combination therapy as compared with controls (fig. S14). The host transcriptional responses among the mock and infected groups were different in principle component analysis (PCA) with samples collected at both 2 and 4 dpi; however, differences among vehicle and treated animals were not readily apparent in those global analyses (fig. S15A). As compared to mock infected animals, hundreds of genes were upregulated in vehicle and antiviral therapy groups (fig. S15B). Upon comparing the patterns of differentially expressed genes of all groups, 131 were uniquely regulated in vehicle treated animals (fig. S15C). Many genes known to play a role in the innate and adaptive immune response (including *Ccl20, Ifna2, IL12rb1, clec4d, Ccl5, Ccl9, H2-Q2/6/7, H2-K2, Irf1,* and *S100a8*,) (fig. S15D) were uniquely upregulated in vehicle-treated animals, which was confirmed by pathway analysis (fig. S16). Thus, effective combination antiviral therapy reduced viral replication, pathogenesis, and the host inflammatory response in the lung.

DISCUSSION

In response to vaccine induced and naturally acquired immunity, the SARS-CoV-2 spike protein has changed extensively, conferring an increased ability to evade immunity and antibody-based countermeasures as we have recently seen with Omicron BA.1 and related sub-lineages (8, 47). Moreover, increasingly immune-evasive variants, such as BQ.1.1 and XBB, can evade all human monoclonal antibodies in clinical use; however, antivirals like remdesivir remain active against these variants (48). Three broad- and direct-acting antivirals (remdesivir, molnupiravir, and nirmatrelvir/ritonavir (Paxlovid)) have gained either full approval or Emergency Use Authorization (EUA) by the Food and Drug Administration (FDA), all of which target highly conserved enzymes required for viral replication and likely reduces the risk of escape relative to viral envelop spike protein directed therapies (13, 19-21). When given early after infection, remdesivir reduced the risk of hospitalization due to COVID-19 (22). Similarly, the initiation of both molnupiravir and Paxlovid therapy is recommended within the first five days of the disease to maximize antiviral activity (49). Consistent with this and our earlier findings with remdesivir and molnupiravir (11, 13), we found that early remdesivir and GS-5245 treatment of SARS-CoV and SARS-CoV-2-infected mice offered the most protection against viral pathogenesis (11, 14). In the setting of continued SARS-CoV-2 spike protein evolution and waning vaccine immunity, it is critical to continue to develop orally bioavailable drugs that target conserved CoV proteins that can broadly inhibit SARS-CoV-2 and its current and future VOCs.

Oral antiviral drugs are needed to treat outpatients with risk factors of developing severe COVID-19 to best ameliorate pathogenesis, lessen the duration of disease, and maximize the potential to prevent hospitalization. Despite the efficacy of remdesivir (22), its widespread use has been limited by the requirement of intravenous administration and the trained medical personnel needed to administer drug in outpatient settings such as infusion centers. Direct oral dosing of the parental nucleoside analog, GS-441524, was shown to result in low bioavailability in non-human primates, and high systemic exposures were necessary for efficacy due to its inefficient metabolism to the active nucleoside triphosphate that

inhibits the viral polymerase (24). To overcome these challenges, an oral prodrug (GS-5245; ODV) of the parent nucleoside GS-441524, was developed (24) to more effectively deliver the parent nucleoside following oral administration. GS-5245, through delivery of systemic GS-441524, ultimately forms the same active nucleoside triphosphate in lung tissue as remdesivir. Here, we show that GS-5245 is highly effective at diminishing replication and disease pathogenesis for enzootic, epidemic, emerging, and pandemic coronaviruses including a highly transmissible SARS-CoV-2 Omicron variant following oral administration. The twice daily 30 mg/kg dose was effective across the different SARS-CoV-2 models and corresponded to daily GS-441524 exposures ranging from 81 to 108 μM.h. This exposure is consistent with both the estimated GS-441524 exposure at efficacious oral doses of GS-5245 in a non-human primate SARS-CoV-2 infection model and the targeted exposures in humans (50). Thus, GS-5245 is potentially an additional oral antiviral for the treatment of outpatients with COVID-19.

For maximal pandemic preparedness, drugs targeting highly conserved viral proteins, like the RdRp, are advantageous as they may retain activity against future VOCs and emerging coronavirus threats. Wild animal reservoirs harbor enzootic viruses related to SARS-CoV, MERS-CoV and SARS-CoV-2, which present a threat to our public health security. Thus, GS-5245 may not only prove to be valuable for treating SARS-CoV-2 infections but could also be deployed to treat infections caused by re-emerging CoVs like MERS-CoV, although dosages may need to be revaluated for its use outside of COVID-19. Despite the high degree of conservation in the RdRp and M^{pro}, coronaviruses can evolve to escape single-agent therapies in a laboratory setting (26, 51). Like HIV-1 antiretroviral therapy, which combines several antivirals targeting different viral proteins, such as protease and polymerase inhibitors (52), similar cocktails of antivirals may be useful in treating COVID-19. Combination therapy may more rapidly suppress viral replication or extend the therapeutic window while also reducing the risk of antiviral resistance that may arise with monotherapy; this is especially important for immunocompromised individuals who can have prolonged viral shedding (53-56). If combination therapy more effectively diminishes acute COVID-19, chronic manifestations of disease such as Post-Acute Sequelae of SARS-CoV-2 infection (PASC), also known as long COVID, may also be less likely to develop (45). Moreover, as SARS-CoV-2 infectious virus rebound following Paxlovid treatment has occurred in patients (57, 58), combination drug intervention strategies may be clinically useful in reducing or eliminating cases of viral rebound.

Despite the observed efficacy of GS-5245 in vivo, our study has limitations. The breadth of protection was only tested in mice and not in additional animal models of coronavirus pathogenesis. Although remdesivir exhibits clinical efficacy across broad patient populations and stages of COVID-19 disease, the evaluation of GS-5245's clinical efficacy is ongoing. The clinical efficacy of GS-5245 may be established based on ongoing controlled, randomized, and powered clinical trials in humans. Similarly, although GS-5245 and nirmatrelvir exhibited enhanced efficacy when tested in combination in SARS-CoV-2-infected mice, the clinical efficacy of GS-5245 in combination with Paxlovid based on properly designed human clinical studies has not yet been established.

In summary, our data in mouse models of emerging CoV infection indicate that GS-5245 may have clinical utility against highly transmissible SARS-CoV-2 variants as well as zoonotic coronaviruses that may emerge in the future. Moreover, GS-5245 demonstrated efficacy against common-cold human alphacoronavirus NL63 and pre-emergent SARS-CoV-related viruses, underlining the broad antiviral efficacy of this drug and its potential use in treating infections with common-cold causing human coronaviruses, which can progress to severe illness in the very young and in older adults (59). The present in vitro and in vivo data provide support toward the clinical evaluation of GS-5245 for the treatment of COVID-19 and exemplifies its potential therapeutic benefit for other coronaviruses with pandemic potential.

MATERIALS AND METHODS

Study Design

The primary goal of this study was to evaluate the potential for GS-5245 (obdeldesivir) to treat emerging CoV infections. Given that SARS-CoV-2 most recently caused the COVID-19 pandemic, we focused much of our work on evaluating GS-5245 in SARS-CoV-2 models. Members of the CoV family have a predilection for spillover into new species to cause new disease. Thus, broad-spectrum antivirals with family wide activity have the potential to be useful to treat the CoV infections of today as well as those of tomorrow. As such, the demonstration of antiviral breadth and retention of antiviral activity across the CoV family was also an important goal of our study. To achieve these goals, we employed the A549-hACE2 cell line and human primary lung epithelial cell cultures (HAE) to evaluate antiviral activity, breadth and cytotoxicity. For A549-hACE2 studies, all conditions were performed in triplicate in two independent studies. For HAE studies, all conditions were performed in triplicate in two separate human donors to account for the potential for human genetic variation to affect infection outcomes. Multiple in vivo models were utilized to determine therapeutic efficacy against pandemic (SARS-CoV-2) and emerging (SARS-CoV, MERS-CoV) CoV. The in vivo efficacy studies in mice were intended to gain the data required to justify testing in humans. Mice were age and sex matched and randomly assigned to groups prior to the start of the study. Group sizes were chosen based on historical data not through sample size calculations and study groups were not blinded from study operators but pathology was scored in a blind manner by a veterinary pathologist. Group sizes were typically 10 animals but deviations from this are listed in the figure legends. Studies were iterative and used to inform improved design of future studies but some dose conditions were repeated. Exclusion criteria for in vivo studies were: If a mouse unexpectedly did not lose weight after infection and their viral lung titers were more than 2 $\log_{10}$ lower the mean of the group, this indicated that infection was inefficient, and all data related to that mouse were censored.

Viruses

Recombinant viruses utilized for in vitro studies, including SARS-CoV Urbani expressing nanoluciferase (SARS-nLuc, nLuc replaces ORF7) and MERS-CoV EMC Strain, SARS-CoV-2 WA/1, bat SARS-related CoV RsSHC014, HCoV-NL63 were created from molecular

cDNA clones as described (60-62) previously. The SARS-CoV-2 Omicron BA.1 isolate was obtained as a gift from Yoshihiro Kawaoka from the University of Wisconsin, Madison.

Mouse strains and infections

Eight-week-old female BALB/c mice were purchased from Envigo (#047). Eight-week-old female K18-humanized ACE2 mice on a C57BL/6 background were purchased from Jackson Laboratory (#034860). 288/330^{++} dipeptidyl peptidase 4 (DPP4) mice were bred at the University of North Carolina at Chapel Hill and were described previously (42). For SARS-CoV-2 infections in BALB/c mice, a mouse-adapted SARS-CoV-2 virus (MA10) was used and mice were infected with 1 x 10^4 PFU intranasally (46). For SARS-CoV infections in BALB/c mice, an intranasal infectious of 1 x 10^4 PFU was used (37). For RsSHC014-CoV and SARS-CoV-2 Omicron (BA.1) infections, K18-hACE2 mice were infected with 1 x 10^4 PFU intranasally. Finally, 288/330^{++} DPP4 mice were infected intranasally with 5 x 10^4 PFU with a mouse-adapted MERS-CoV (maM35c4) virus as described previously (41, 42). Infected mice were weighed daily and were monitored for signs of disease in all infection and treatment studies.

GS-5245, molnupiravir, and nirmatrelvir formulations

GS-5245 was synthesized at Gilead Sciences, Inc., and their chemical composition and purity was quality controlled by nuclear magnetic resonance, high resolution mass spectrometry, and high-performance liquid chromatography. Molnupiravir was purchased from MedChemExpress. Nirmatrelvir (PF-07321332) was purchased from MedChemExpress or WuXi AppTec. GS-5245 was solubilized in 2.5% dimethyl sulfoxide, 10% Kolliphor HS-15; 10% Labrasol; 2.5% propylene glycol; 75% water; pH 2-3 for mouse in vivo studies. Molnupiravir was solubilized in 2.5% Kolliphor RH 40, 10% polyethylene glycol, and 87.5% water for mouse in vivo studies. Nirmatrelvir was formulated in 10% ethanol and 90% propylene glycol. Oral antiviral drugs were made available to UNC Chapel Hill under an existing material transfer agreement with Gilead Sciences, Inc.

Structural analysis of nsp12 conservation

A model of the pre-incorporation state of the GS-5245 active metabolite in the SARS-CoV-2 polymerase complex was based on the cryo-EM structure 6XEZ (63) and was previously described (30). Homology models using Schrödinger Release 2022-2 (Prime, Schrödinger, LLC) were generated for the nsp12 subunit were generated for the viral strains used in this study.

Mouse GS-5245 pharmacokinetic studies

Mouse pharmacokinetic (PK) studies were performed at LabCorp Drug Development. Briefly, n=4 female BALB/c mice and n=3 female and n=3 male mice from each different strain of K18-hACE2 and 288/330^{++} DPP4 were dosed with 30 mg/kg of GS-5245 by oral gavage. Plasma concentrations (μM) of GS-411524 were quantitated in each mouse strain at select timepoints over 24 hr as described previously (31).

Antiviral activity of GS-5245 against SARS-CoV-2

We employed an antiviral assay as described (31). Briefly, the human lung epithelial cell line A549 (based on ATCC # CCL185) stably expressing hACE2 (BEI # NR-53821) was plated at a density of 20,000 cells per well in 100 μL in black-walled clear-bottom 96-well plates 24 hr prior to infection. GS-5245, GS-441524, remdesivir, and nirmatrelvir were diluted in 100% DMSO (1:2) resulting in a 1000X dose response from 10 to 0.039 μM. All conditions were performed in triplicate. In a Biosafety Level 3 Laboratory (BSL3), culture medium (Dulbecco's Modified Eagle's Medium (DMEM), 10% fetal bovine serum (FBS), 1X antibiotic/antimycotic (A/A)). was removed and cells were infected with 100 μL SARS-CoV-2 nLUC (multiplicity of infection (MOI) = 0.5) for 1 hr at 37 °C. After this incubation, virus was removed and wells were washed (150 μL) with infection media (DMEM, 4% FBS, 1X A/A). Infection media (100 μL) containing diluted drug in dose response was then added. DMSO remained at 0.1% across the dilution series. Plates were incubated at 37 °C for 48 hr. NanoGlo assay was performed at 48 hpi. Sibling plates that were exposed to drug but not infected were used to gauge cytotoxicity using a CellTiter-Glo assay (CTG, Promega) at 48 hr post treatment. Values were normalized to the uninfected and infected DMSO controls (0% and 100% infection, respectively). Data were fit using a four-parameter non-linear regression analysis using GraphPad Prism. EC_{50} and CC_{50} (Cytotoxic concentration at which 50% of cells are viable) values were then determined as the concentration reducing the signal by 50%.

Antiviral activity of GS-5245 against HCoV-NL63

An antiviral assay was performed with recombinant NL63 reporter virus expressing nanoluciferase as described (64). Briefly, LLCMK2 cells stably expressing TMPRSS2 were seeded at 20,000 cells per well in culture medium (DMEM, 10% FBS, 1X non-essential amino acids (NEAA), 1X penicillin/streptomycin (P/S)) and infected with NL63 nLUC diluted in infection medium (DMEM, 5% FBS, 1X NEAA, 1X P/S) at an MOI of 0.02 for 1 hr after which virus was removed. Cultures were then washed with infection medium and a dose response of each drug diluted in infection medium was added in triplicate. After 48 hr, virus replication was quantitated by measuring nanoluciferase expression. For cytotoxicity, uninfected sibling plates were exposed to the same dose response as those infected. Cytotoxicity was quantitated using CellTiter Glo assay at 48 hr post exposure. Three independent studies were performed. Values were normalized to the uninfected and infected DMSO controls (0% and 100% infection, respectively). Data was fit using a four-parameter non-linear regression analysis using GraphPad Prism. EC_{50} and CC_{50} values were then determined as the concentration reducing the signal by 50%.

Antiviral activity in primary human airway epithelial cells

Human airway epithelial (HAE) cell cultures were obtained from the Tissue Procurement and Cell Culture Core Laboratory in the Marsico Lung Institute/Cystic Fibrosis Research Center at UNC. Prior to infection, HAE were washed with PBS and moved into ALI media (Custom media from UNC Marsico Lung Institute Tissue Procurement and Cell Culture Core) containing a dose response of 10, 1, or 0.1μM GS-5245 or DMSO. HAE were infected at an MOI of 0.5 for 1.5 hr at 37°C after which virus was removed. Cultures were

washed with PBS and then incubated at 37°C for 72hr. Virus titration was performed by plaque assay as previously described (46). Cells from two different patient donors (sex of origin unknown) were utilized for the above studies to control for variation driven by host genetics. Cytotoxicity was measured using a ToxiLight Assay (Lonza) in triplicate HAE cell cultures treated with 10, 1, or 0.1μM GS-5245 or DMSO. DMSO remained at 0.1% for all conditions. As a positive control, duplicate wells were exposed to Promega nanoluciferase lysis buffer for 10 minutes prior to Toxilight Assay.

Animal care

Animal efficacy studies were performed in accordance with the recommendations for care and use of animals by the Office of Laboratory Animal Welfare (OLAW), National Institutes of Health and the Institutional Animal Care and Use Committee (IACUC) protocol number: 20-059 and 22-077 at University of North Carolina (UNC permit no. A-3410-01). All mice were anesthetized prior to viral inoculation and efforts were undertaken to reduce animal suffering. Mice were fed standard chow diets and housed in groups of five.

Lung pathology and scoring

After euthanasia, the left lung lobe was harvested and fixed in 10% phosphate buffered formalin for at least 7 days after which tissues were processed on a Leica ASP 6025, embedded in paraffin (Leica Paraplast) and sectioned at 4um thickness. Sequential sections were stained with hematoxylin and eosin (Richard Allan Scientific) or stained for SARS-CoV-2 nucleocapsid using a monoclonal anti-SARS-CoV nucleocapsid antibody (NB100-56576, RRID: AB_838838, Novus Biologicals) on the Ventana Discovery platform (Roche). Antigen retrieval was performed using Ventana's CC1 (pH 8.5), tissues were blocked, primary antibody diluted at 1:250 using Discovery Casein Diluent (760-219, Roche), ready-to use secondary antibody (Discovery OmniMap anti Rabbit HRP, 760-4311), followed by DAB development and Hematoxylin II staining. Acute lung injury was quantified with two distinct lung pathology scoring tools. The first scoring tool is the Matute-Bello scoring system developed by the American Thoracic Society (ATS), and the second scoring tool is the Diffuse Alveolar Damage (DAD) to score lung damage caused by acute viral infections as described previously (14). Lung scoring and scoring analyses were performed by a Board-Certified Veterinary Pathologist who was blinded to the treatment groups. Lung pathology slides were read and scored at 600X total magnification.

Laboratory biosafety

Cell culture and animal virology studies were approved by the UNC Institutional Biosafety Committee approved under laboratory and animal protocols used in the Baric laboratory. All work described here, including coronavirus work, was performed with approved standard operating procedures for SARS-CoV, SARS-CoV-2, and MERS-CoV in a BSL3 facility which met requirements recommended in "Biosafety in Microbiological and Biomedical Laboratories", by the U.S. Department of Health and Human Service, the U.S. Public Health Service, and the U.S. Center for Disease Control and Prevention (CDC), and the National Institutes of Health (NIH).

RNA extraction, sequencing, and analysis

Total RNA was isolated from lung lobes homogenized in Trizol reagent (Thermo) using Qiagen RNeasy kit according to protocol. Illumina total RNA-sequencing was performed by the UNC High Throughput Sequencing Facility (HTSF). Total RNA libraries were prepared (Kapa total RNA with Ribo Erase) and read on the Illumina NovaSeq6000 platform (paired end 2X100). Analysis of RNA-sequencing data was carried out using R in R Studio, as previously described(65). The following repository of publicly available code was utilized for our analysis: https://github.com/DIYtranscriptomics/DIYtranscriptomics.github.io/tree/master/Code/files. Briefly, raw reads were mapped to the mouse reference transcriptome using Kallisto. Quantification of transcripts were normalized using the TMM method in EdgeR, and differentially expressed genes (p. Adj.val <0.01; logFC > 2.5) were identified using linear modeling with Limma. Gene ontology analysis was carried out using Ingenuity IPA. Heatmaps were produced using the Broad Institute's Morpheus web application (https://software.broadinstitute.org/morpheus/). Raw data can be found at NCBI GEO accession GSE254256.

STATISTICAL ANALYSIS

Raw data for all quantitative figures are provided in Data File S1. The statistical analysis performed using Prism 9, SAS Software version 9.4 (SAS Institute Inc.) or the R statistical package version 3.6.1. Statistical tests used are described in the figure legends.

Supplementary Material

Refer to Web version on PubMed Central for supplementary material.

FUNDING

This work was supported by an NIAID AVIDD U19AI171292 to R.S.B and T.P.S., R01 AI132178 and R01AI132178-04S1 to T.P.S. and R.S.B., an NIH animal models contract (HHSN272201700036I) to R.S.B, and The North Carolina Policy Collaboratory at University of North Carolina at Chapel Hill with funding from the North Carolina Coronavirus Relief Fund established and appropriated by the North Carolina General Assembly to R.S.B and T.P.S. The Pathology Services Core at the University of North Carolina-Chapel Hill is supported in part by an NCI Center Core Support Grant (5P30CA016080-42). D.R.M. is funded by a Hanna H. Gray Fellowship from the Howard Hughes Medical Institute.

DATA AVAILABILITY

All data associated with this study are in the paper or supplementary materials. Material and reagents generated in this study, except those created by Gilead Sciences and those available through BEI (Biodefense and Emerging Infections Research Resources Repository) Resources, will be made available upon installment of a standard material transfer agreement (MTA) through UNC. The following viruses and reagents are currently available through BEI Resources: SARS-CoV-2 MA10, SARS-CoV-2 nLUC, and A549-hACE2 cells.

REFERENCES AND NOTES

1. Walls AC et al. , Elicitation of broadly protective sarbecovirus immunity by receptor-binding domain nanoparticle vaccines. Cell 184, 5432–5447.e5416 (2021). [PubMed: 34619077]
2. Saunders KO et al. , Neutralizing antibody vaccine for pandemic and pre-emergent coronaviruses. Nature, (2021).
3. Martinez DR et al. , Chimeric spike mRNA vaccines protect against Sarbecovirus challenge in mice. Science 373, 991–998 (2021). [PubMed: 34214046]
4. Martinez DR et al. , A broadly cross-reactive antibody neutralizes and protects against sarbecovirus challenge in mice. Sci Transl Med 14, eabj7125 (2022). [PubMed: 34726473]
5. Rappazzo CG et al. , Broad and potent activity against SARS-like viruses by an engineered human monoclonal antibody. Science 371, 823–829 (2021). [PubMed: 33495307]
6. Pinto D et al. , Cross-neutralization of SARS-CoV-2 by a human monoclonal SARS-CoV antibody. Nature 583, 290–295 (2020). [PubMed: 32422645]
7. Tortorici MA et al. , Broad sarbecovirus neutralization by a human monoclonal antibody. Nature 597, 103–108 (2021). [PubMed: 34280951]
8. Cameroni E et al. , Broadly neutralizing antibodies overcome SARS-CoV-2 Omicron antigenic shift. Nature 602, 664–670 (2022). [PubMed: 35016195]
9. Brown AJ et al. , Broad spectrum antiviral remdesivir inhibits human endemic and zoonotic deltacoronaviruses with a highly divergent RNA dependent RNA polymerase. Antiviral Res 169, 104541 (2019). [PubMed: 31233808]
10. Pruijssers AJ et al. , Remdesivir Inhibits SARS-CoV-2 in Human Lung Cells and Chimeric SARS-CoV Expressing the SARS-CoV-2 RNA Polymerase in Mice. Cell Rep 32, 107940 (2020). [PubMed: 32668216]
11. Sheahan TP et al. , Broad-spectrum antiviral GS-5734 inhibits both epidemic and zoonotic coronaviruses. Sci Transl Med 9, (2017).
12. Sheahan TP et al. , Comparative therapeutic efficacy of remdesivir and combination lopinavir, ritonavir, and interferon beta against MERS-CoV. Nat Commun 11, 222 (2020). [PubMed: 31924756]
13. Sheahan TP et al. , An orally bioavailable broad-spectrum antiviral inhibits SARS-CoV-2 in human airway epithelial cell cultures and multiple coronaviruses in mice. Sci Transl Med 12, (2020).
14. Martinez DR et al. , Prevention and therapy of SARS-CoV-2 and the B.1.351 variant in mice. Cell Rep 36, 109450 (2021). [PubMed: 34289384]
15. Williamson BN et al. , Clinical benefit of remdesivir in rhesus macaques infected with SARS-CoV-2. Nature, (2020).
16. Pitts J et al. , Remdesivir and GS-441524 Retain Antiviral Activity against Delta, Omicron, and Other Emergent SARS-CoV-2 Variants. Antimicrob Agents Chemother 66, e0022222 (2022). [PubMed: 35532238]
17. Beigel JH et al. , Remdesivir for the Treatment of Covid-19 - Final Report. N Engl J Med 383, 1813–1826 (2020). [PubMed: 32445440]
18. Jayk Bernal A et al. , Molnupiravir for Oral Treatment of Covid-19 in Nonhospitalized Patients. New England Journal of Medicine 386, 509–520 (2021). [PubMed: 34914868]
19. Owen DR et al. , An oral SARS-CoV-2 M(pro) inhibitor clinical candidate for the treatment of COVID-19. Science 374, 1586–1593 (2021). [PubMed: 34726479]
20. Hammond J et al. , Oral Nirmatrelvir for High-Risk, Nonhospitalized Adults with Covid-19. New England Journal of Medicine, (2022).
21. Fischer WA 2nd et al. , A phase 2a clinical trial of molnupiravir in patients with COVID-19 shows accelerated SARS-CoV-2 RNA clearance and elimination of infectious virus. Sci Transl Med 14, eabl7430 (2022). [PubMed: 34941423]
22. Gottlieb RL et al. , Early Remdesivir to Prevent Progression to Severe Covid-19 in Outpatients. New England Journal of Medicine 386, 305–315 (2021). [PubMed: 34937145]
23. Vangeel L et al. , Remdesivir, Molnupiravir and Nirmatrelvir remain active against SARS-CoV-2 Omicron and other variants of concern. Antiviral Res 198, 105252 (2022). [PubMed: 35085683]

24. Mackman RL et al. , Discovery of GS-5245 (Obeldesivir), an Oral Prodrug of Nucleoside GS-441524 That Exhibits Antiviral Efficacy in SARS-CoV-2-Infected African Green Monkeys. J Med Chem 66, 11701–11717 (2023). [PubMed: 37596939]
25. Gordon CJ et al. , Remdesivir is a direct-acting antiviral that inhibits RNA-dependent RNA polymerase from severe acute respiratory syndrome coronavirus 2 with high potency. J Biol Chem 295, 6785–6797 (2020). [PubMed: 32284326]
26. Stevens LJ et al. , Mutations in the SARS-CoV-2 RNA dependent RNA polymerase confer resistance to remdesivir by distinct mechanisms. Sci Transl Med, eabo0718 (2022). [PubMed: 35482820]
27. Tchesnokov EP, Feng JY, Porter DP, Gotte M, Mechanism of Inhibition of Ebola Virus RNA-Dependent RNA Polymerase by Remdesivir. Viruses 11, (2019).
28. Fulcher ML, Randell SH, Human nasal and tracheo-bronchial respiratory epithelial cell culture. Methods Mol Biol 945, 109–121 (2013). [PubMed: 23097104]
29. Malone BF et al. , Structural basis for substrate selection by the SARS-CoV-2 replicase. Nature 614, 781–787 (2023). [PubMed: 36725929]
30. Gordon CJ et al. , Efficient incorporation and template-dependent polymerase inhibition are major determinants for the broad-spectrum antiviral activity of remdesivir. J Biol Chem 298, 101529 (2022). [PubMed: 34953856]
31. Schäfer A et al. , Therapeutic treatment with an oral prodrug of the remdesivir parental nucleoside is protective against SARS-CoV-2 pathogenesis in mice. Sci Transl Med 14, eabm3410 (2022). [PubMed: 35315683]
32. Leist SR et al. , A Mouse-Adapted SARS-CoV-2 Induces Acute Lung Injury and Mortality in Standard Laboratory Mice. Cell 183, 1070–1085 e1012 (2020). [PubMed: 33031744]
33. Menachery VD et al. , A SARS-like cluster of circulating bat coronaviruses shows potential for human emergence. Nat Med 21, 1508–1513 (2015). [PubMed: 26552008]
34. Zhong NS et al. , Epidemiology and cause of severe acute respiratory syndrome (SARS) in Guangdong, People's Republic of China, in February, 2003. Lancet 362, 1353–1358 (2003). [PubMed: 14585636]
35. Peiris JSM, Yuen KY, Osterhaus ADME, Stöhr K, The Severe Acute Respiratory Syndrome. New England Journal of Medicine 349, 2431–2441 (2003). [PubMed: 14681510]
36. Menachery VD et al. , SARS-like WIV1-CoV poised for human emergence. Proc Natl Acad Sci U S A 113, 3048–3053 (2016). [PubMed: 26976607]
37. Roberts A et al. , A mouse-adapted SARS-coronavirus causes disease and mortality in BALB/c mice. PLoS Pathog 3, e5 (2007). [PubMed: 17222058]
38. Liljander A et al. , MERS-CoV Antibodies in Humans, Africa, 2013-2014. Emerg Infect Dis 22, 1086–1089 (2016). [PubMed: 27071076]
39. Muller MA et al. , Presence of Middle East respiratory syndrome coronavirus antibodies in Saudi Arabia: a nationwide, cross-sectional, serological study. Lancet Infect Dis 15, 629 (2015).
40. Corman VM et al. , Link of a ubiquitous human coronavirus to dromedary camels. Proc Natl Acad Sci U S A 113, 9864–9869 (2016). [PubMed: 27528677]
41. Douglas MG, Kocher JF, Scobey T, Baric RS, Cockrell AS, Adaptive evolution influences the infectious dose of MERS-CoV necessary to achieve severe respiratory disease. Virology 517, 98–107 (2018). [PubMed: 29277291]
42. Cockrell AS et al. , A mouse model for MERS coronavirus-induced acute respiratory distress syndrome. Nat Microbiol 2, 16226 (2016). [PubMed: 27892925]
43. Halfmann PJ et al. , SARS-CoV-2 Omicron virus causes attenuated disease in mice and hamsters. Nature, (2022).
44. Seifert M et al. , Inhibition of SARS-CoV-2 polymerase by nucleotide analogs from a single-molecule perspective. Elife 10, (2021).
45. Dinnon KH 3rd et al. , SARS-CoV-2 infection produces chronic pulmonary epithelial and immune cell dysfunction with fibrosis in mice. Sci Transl Med, eabo5070 (2022). [PubMed: 35857635]
46. Leist SR et al. , A Mouse-Adapted SARS-CoV-2 Induces Acute Lung Injury and Mortality in Standard Laboratory Mice. Cell 183, 1070–1085.e1012 (2020). [PubMed: 33031744]

47. Yu J et al. , Neutralization of the SARS-CoV-2 Omicron BA.1 and BA.2 Variants. N Engl J Med 386, 1579–1580 (2022). [PubMed: 35294809]
48. Imai M et al. , Efficacy of Antiviral Agents against Omicron Subvariants BQ.1.1 and XBB. New England Journal of Medicine, (2022).
49. CDC, Interim Clinical Considerations for COVID-19 Treatment in Outpatients. (2024).
50. Mackman RL et al. , Discovery of GS-5245 (Obeldesivir), an Oral Prodrug of Nucleoside GS-441524 that Exhibits Antiviral Efficacy in SARS-CoV-2 Infected African Green Monkeys. bioRxiv, 2023.2004.2028.538473 (2023).
51. Szemiel AM et al. , In vitro selection of Remdesivir resistance suggests evolutionary predictability of SARS-CoV-2. PLoS Pathog 17, e1009929 (2021). [PubMed: 34534263]
52. Hammer SM et al. , A controlled trial of two nucleoside analogues plus indinavir in persons with human immunodeficiency virus infection and CD4 cell counts of 200 per cubic millimeter or less. AIDS Clinical Trials Group 320 Study Team. N Engl J Med 337, 725–733 (1997). [PubMed: 9287227]
53. Gandhi S et al. , De novo emergence of a remdesivir resistance mutation during treatment of persistent SARS-CoV-2 infection in an immunocompromised patient: a case report. Nat Commun 13, 1547 (2022). [PubMed: 35301314]
54. Hogan JI et al. , Remdesivir Resistance in Transplant Recipients With Persistent Coronavirus Disease 2019. Clinical Infectious Diseases 76, 342–345 (2022).
55. Heyer A et al. , Remdesivir-induced emergence of SARS-CoV2 variants in patients with prolonged infection. Cell Rep Med 3, 100735 (2022). [PubMed: 36075217]
56. Heilmann E et al. , SARS-CoV-2 3CL(pro) mutations selected in a VSV-based system confer resistance to nirmatrelvir, ensitrelvir, and GC376. Sci Transl Med 15, eabq7360 (2023). [PubMed: 36194133]
57. Carlin AF et al. , Virologic and Immunologic Characterization of COVID-19 Recrudescence after Nirmatrelvir/Ritonavir Treatment. Clin Infect Dis, (2022).
58. Boucau J et al. , Characterization of virologic rebound following nirmatrelvir-ritonavir treatment for COVID-19. Clin Infect Dis, (2022).
59. Kesheh MM, Hosseini P, Soltani S, Zandi M, An overview on the seven pathogenic human coronaviruses. Rev Med Virol 32, e2282 (2022). [PubMed: 34339073]
60. Sims AC et al. , Severe acute respiratory syndrome coronavirus infection of human ciliated airway epithelia: role of ciliated cells in viral spread in the conducting airways of the lungs. J Virol 79, 15511–15524 (2005). [PubMed: 16306622]
61. Hou YJ et al. , SARS-CoV-2 Reverse Genetics Reveals a Variable Infection Gradient in the Respiratory Tract. Cell 182, 429–446.e414 (2020). [PubMed: 32526206]
62. Scobey T et al. , Reverse genetics with a full-length infectious cDNA of the Middle East respiratory syndrome coronavirus. Proc Natl Acad Sci U S A 110, 16157–16162 (2013). [PubMed: 24043791]
63. Chen J et al. , Structural Basis for Helicase-Polymerase Coupling in the SARS-CoV-2 Replication-Transcription Complex. Cell 182, 1560–1573.e1513 (2020). [PubMed: 32783916]
64. Edwards CE et al. , Swine acute diarrhea syndrome coronavirus replication in primary human cells reveals potential susceptibility to infection. Proc Natl Acad Sci U S A 117, 26915–26925 (2020). [PubMed: 33046644]
65. Brown AJ et al. , Host genetic variation guides hepacivirus clearance, chronicity, and liver fibrosis in mice. Hepatology, (2023).

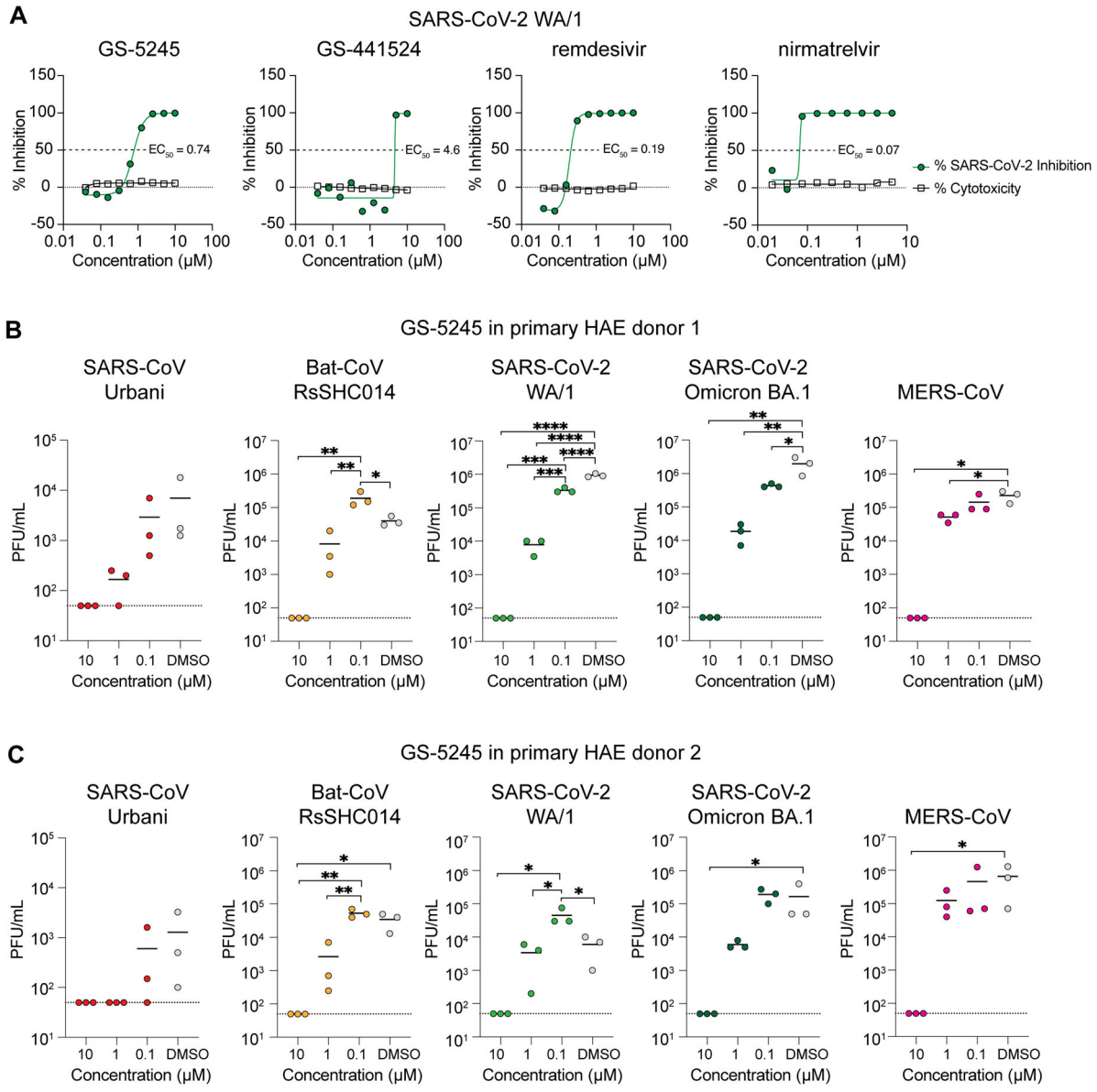

Fig. 1. GS-5245 is broadly active against a panel of enzootic, endemic and pandemic coronaviruses in primary human airway cells.

(A) The mean percent inhibition and cytotoxicity of SARS-CoV-2 WA/1 replication by GS-5245 and control compounds GS-441524, remdesivir, and nirmatrelvir in A459-hACE2 cells is shown (triplicate samples were analyzed). Cells were infected at an MOI of 0.5. Data are representative of two independent experiments. **(B)** Antiviral activity of GS-5245 is shown for primary human airway epithelial cells from donor 1 against SARS-CoV and related bat-CoV SHC014, SARS-CoV-2 WA1 and SARS-CoV-2 Omicron BA.1 and MERS-CoV. HAEs were treated with indicated doses of drug or DMSO and then infected at an MOI of 0.5. At 2 hpi, input virus was removed, cultures were washed once, and infectious virus titers in plaque forming units (PFU) was measured in apical washes at 72 hpi. Cultures remained in the presence of drug for the duration of the study. **(C)** Antiviral activity of GS-5245 in primary human airway epithelial cell from donor 2 against SARS-CoV and

related bat-CoV SHC014, SARS-CoV-2 WA1, and SARS-CoV-2 Omicron BA.1 and MERS-CoV. This was performed similarly but independent of the study in (B). For (B and C), each symbol represents the virus titer per triplicate culture and the line is at the mean and asterisks indicate statistical significance as determined by One-Way ANOVA with Tukey's multiple comparison test where * $p \leq 0.05$, ** $p \leq 0.01$, *** $p \leq 0.001$, **** $p \leq 0.0001$. The dashed lines in (A) denote the IC_{50} values. The dashed lines in (B and C) denote the lower limit of detection.

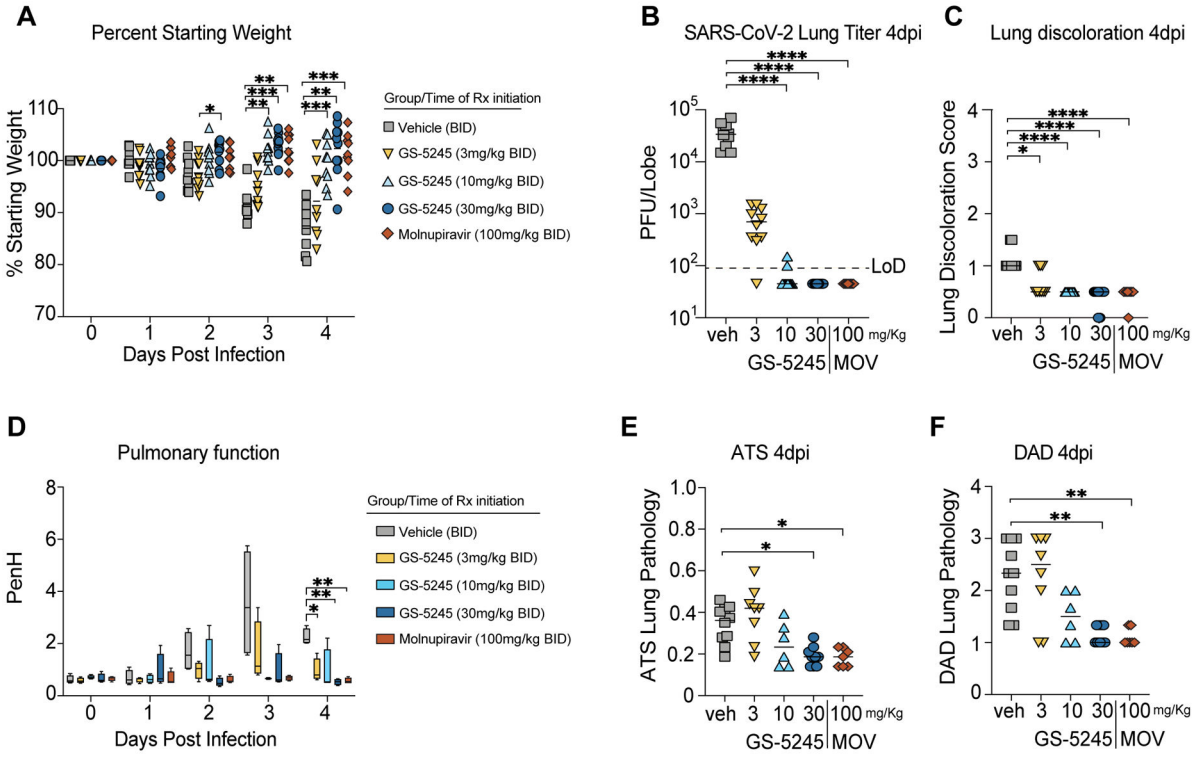

Fig. 2. GS-5245 exhibits dose-dependent therapeutic efficacy against SARS-CoV-2 MA10 in BALB/c mice.

(A) Shown is the percent change compared with starting weight in 10-week-old female BALB/c mice infected with SARS-CoV-2 MA10 at 1 x 10^4 PFU. Mice were treated BID with vehicle, 3 mg/kg GS-5245, 10 mg/kg GS-5245, 30 mg/kg GS-5245, or 100 mg/kg molnupiravir starting at 12 hpi. n = 10 mice per group. Rx = drug. **(B)** SARS-CoV-2 MA10 lung infectious viral titers were measured at 4 dpi in mice treated with vehicle (veh), GS-5245 at increasing concentrations, or 100 mg/kg molnupiravir (MOV). LOD, limit of detection. **(C)** Macroscopic lung discoloration was evaluated at 4 dpi in therapeutically treated mice compared to vehicle. **(D)** Pulmonary function (PenH) was monitored by whole-body plethysmography from day zero through 4 dpi in SARS-CoV-2-infected treated mice. The boxes encompass the 25th to 75th percentile, whereas the whiskers represent the range. **(E)** Microscopic ATS acute lung injury pathology scoring at 4 dpi is shown for vehicle, GS-5245, and molnupiravir-treated mice. **(F)** Microscopic DAD acute lung injury pathology scoring at 4 dpi is shown for vehicle, GS-5245, and molnupiravir-treated mice. For (A), (B), (C), (E) and (F), each symbol represents data for one mouse and the line is at the mean. For (A and D), asterisks denote significant p values from a two-way ANOVA after a Tukey's multiple comparisons test where * $p \leq 0.05$, ** $p \leq 0.01$, *** $p \leq 0.001$, **** $p \leq 0.0001$. For (B), (C), (E) and (F), asterisks denote significant p values from a Kruskal-Wallis test after a Dunn's multiple comparisons test where * $p \leq 0.05$, ** $p \leq 0.01$, **** $p \leq 0.0001$. This study was performed once but some conditions were repeated in fig. S8 and S9.

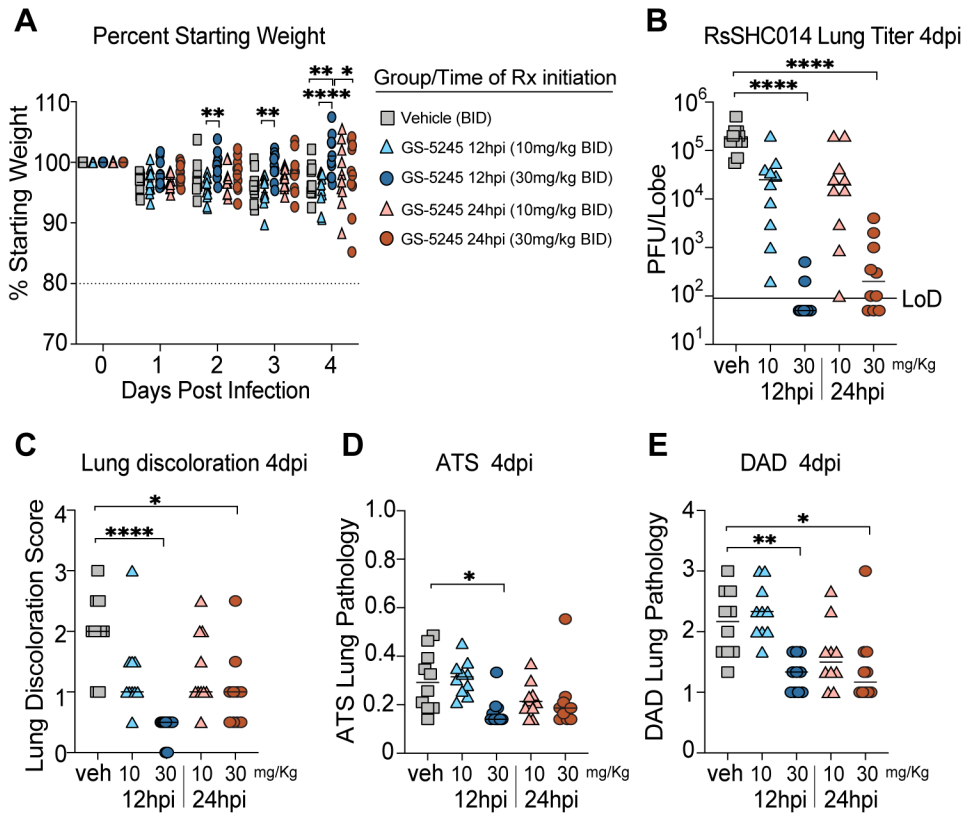

Fig. 3. Therapeutic efficacy of GS-5245 against pre-emergent bat SARS-related RsSHC014-CoV in K18-hACE2 mice.

(A) Shown is the percent change compared with starting weight in 10-week-old female K18-hACE2 mice infected with RsSHC014-CoV at 1 x 10^4 PFU. Mice were treated BID with vehicle, 10 mg/kg GS-5245, 30 mg/kg GS-5245 at 12 hpi or 24 hpi. n = 10 mice per group. Asterisks denote significant p values from a two-way ANOVA after a Tukey's multiple comparisons test where * $p \leq 0.05$, ** $p \leq 0.01$, **** $p \leq 0.0001$. **(B)** RsSHC014-CoV lung infectious viral titers were measured 4 dpi in mice treated with vehicle (veh) or GS-5245 at 10 and 30 mg/kg at either 12 or 24 hpi. LOD = limit of detection. **(C)** Macroscopic lung discoloration was evaluated at 4 dpi in therapeutically treated K18-hACE2 mice compared to vehicle. **(D)** Microscopic ATS acute lung injury pathology scoring at 4 dpi is shown for vehicle vs. GS-5245-treated mice. **(E)** Microscopic DAD acute lung injury pathology scoring at 4 dpi is shown for vehicle vs. GS-5245-treated mice. For all panels, each symbol represents data for one mouse and the line is at the mean. For (B), (C), (D) and (E), Asterisks denote significant p values from a Kruskal-Wallis test after a Dunn's multiple comparisons test where * $p \leq 0.05$, ** $p \leq 0.01$, **** $p \leq 0.0001$. This study was performed once.

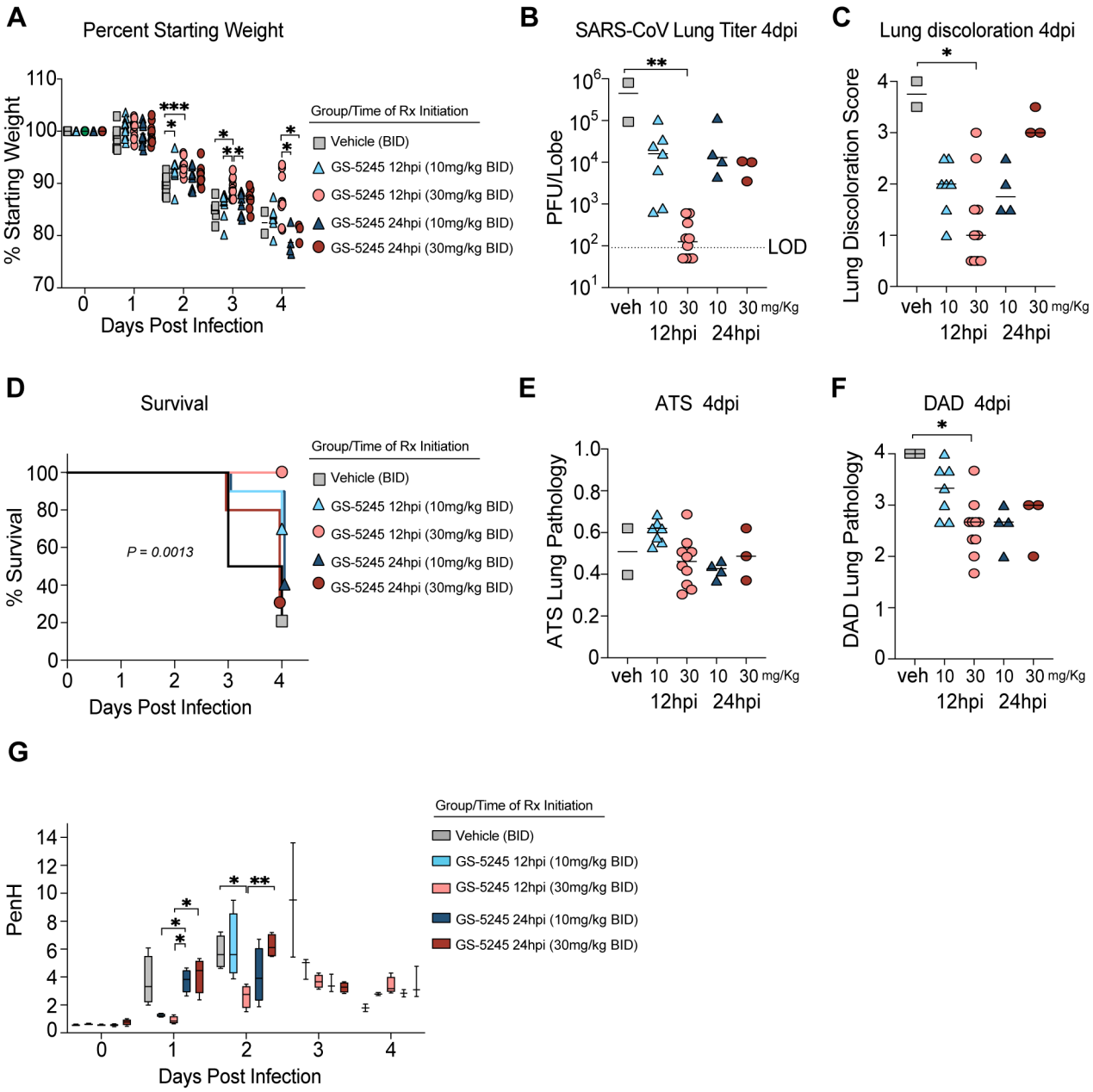

Fig. 4. GS-5245 protects against SARS-CoV MA15 mortality in BALB/c mice.

(A) Shown is the percent change compared with starting weight in 10-week-old female BALB/c mice infected with SARS-CoV MA15 at 1 x 10^4 PFU . Mice were treated BID with vehicle, 10 mg/kg GS-5245, 30 mg/kg GS-5245 at 12 hpi or at 24 hpi. n = 10 mice per group. **(B)** SARS-CoV MA15 lung infectious viral titers were measured 4 dpi in mice treated with vehicle or GS-5245 at 10 and 30 mg/kg at either 12 or 24 hpi. **(C)** Macroscopic lung discoloration at 4 dpi is shown for therapeutically treated BALB/c mice compared to vehicle. **(D)** Shown is the percent survival in vehicle vs GS-5245-treated mice. Survival curves are different (p = 0.0013) using a Log-rank Mantel-Cox test. **(E)** Microscopic ATS acute lung injury pathology scoring at 4 dpi is shown for vehicle vs. GS-5245-treated mice.

(F) Microscopic DAD acute lung injury pathology scoring at 4 dpi is shown for vehicle vs. GS-5245-treated mice. **(G)** Shown is pulmonary function monitored by whole-body plethysmography from day zero through 4 dpi in SARS-CoV-infected treated mice. The boxes encompass the 25th to 75th percentile, whereas the whiskers represent the range. For (A), (B), (C), (E) and (F), each symbol represents data for one mouse and the line is at the mean. For (A) and (G), asterisks denote significant p values from a mixed-effects analysis (REML) with a Tukey's multiple comparisons test where * $p \leq 0.05$, ** $p \leq 0.01$, *** $p \leq 0.001$. For (B), (C), (E), and (F), asterisks denote significant p values from a Kruskal-Wallis test after a Dunn's multiple comparisons test where * $p \leq 0.05$, ** $p \leq 0.01$. This study was performed once.

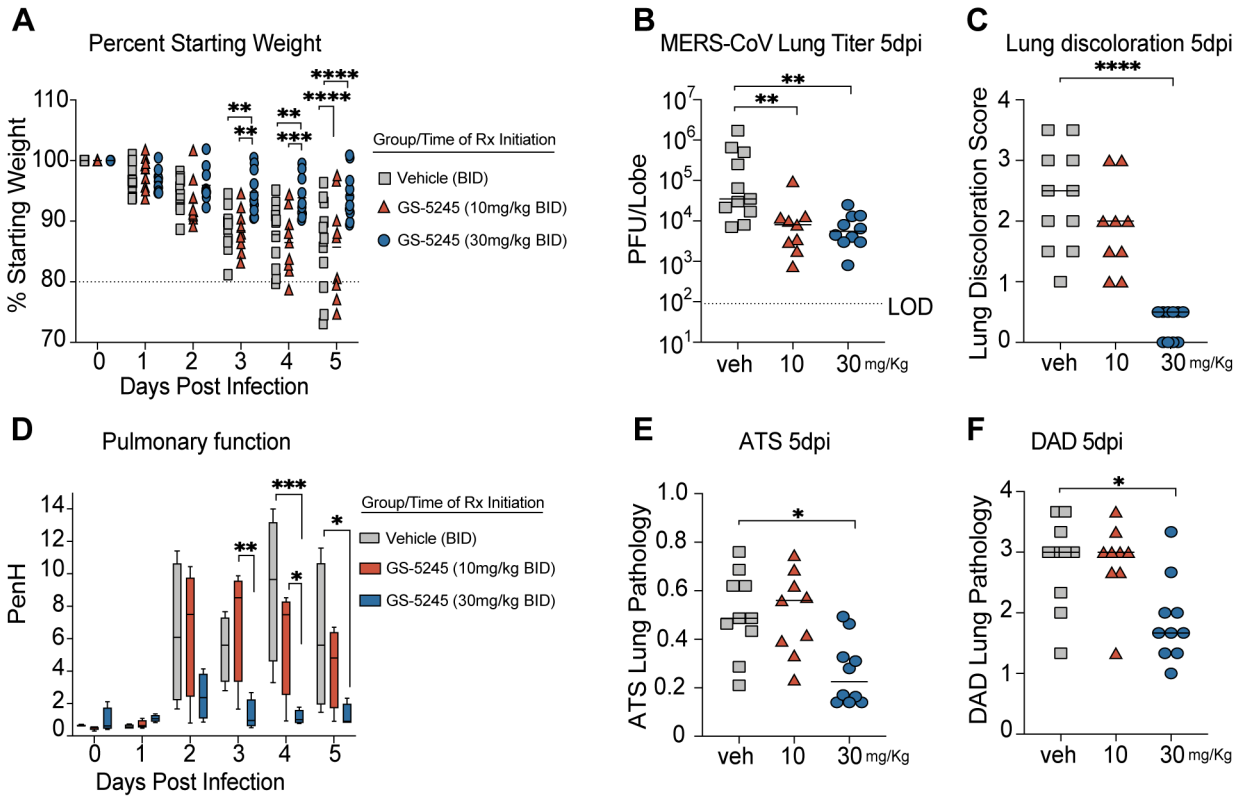

Fig. 5. GS-5245 therapy protects against MERS-CoV pathogenesis in mice.

(A) Shown is the percent change compared with starting weight in 20-week-old male and female 288/330^{++} DPP4-modified mice infected with a mouse-adapted MERS-CoV at 5 x 10^4 PFU. Mice were treated BID starting at 12 hpi with vehicle, 10 mg/kg GS-5245, or 30 mg/kg GS-5245. n = 8 total mice per group. Male and female mice were distributed as equally as possible in each group. **(B)** MERS-CoV lung infectious viral titers were measured at 5 dpi in mice treated with vehicle or GS-5245 at 10 and 30 mg/kg at 12 hpi. **(C)** Macroscopic lung discoloration at 5 dpi is shown for therapeutically treated mice compared to vehicle. **(D)** Shown is pulmonary function monitored by whole-body plethysmography from day 0 through 5 dpi in MERS-CoV-infected treated 288/330^{++} DPP4 mice. The boxes encompass the 25th to 75th percentile, whereas the whiskers represent the range. **(E)** Microscopic ATS acute lung injury pathology scoring at 5 dpi is shown for vehicle vs. GS-5245-treated mice. **(F)** Microscopic DAD acute lung injury pathology scoring at 5 dpi is shown for vehicle vs. GS-5245-treated mice. For (A), (B), (C), (E) and (F), each symbol represents data for one mouse and the line is at the mean. For (A) and (D), asterisks denote significant p values from a two-way ANOVA after a Tukey's multiple comparisons test where * $p \leq 0.05$, ** $p \leq 0.01$, *** $p \leq 0.001$, **** $p \leq 0.0001$. For (B), (C), (E) and (F), asterisks denote significant p values from a Kruskal-Wallis test after a Dunn's multiple comparisons test where * $p \leq 0.05$, ** $p \leq 0.01$, **** $p \leq 0.0001$. This study was performed once.

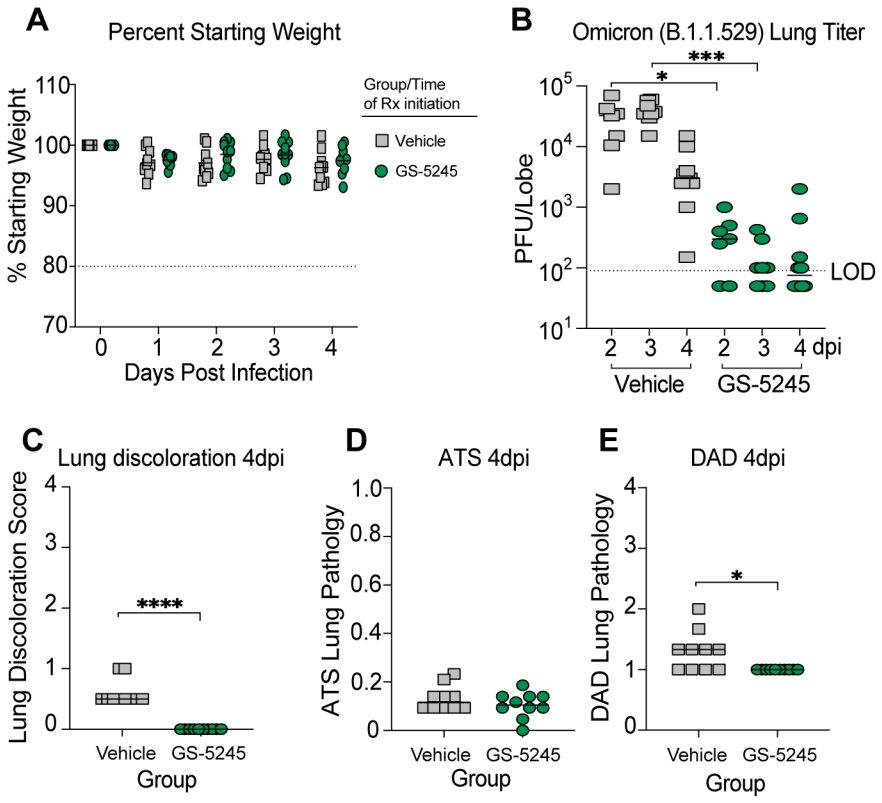

Fig. 6. GS-5245 therapy potently reduces SARS-CoV-2 Omicron replication in K18-hACE2 mice.

(A) Shown is the percent change compared with starting weight in 10-week-old female K18-hACE2 mice infected with a SARS-CoV-2 Omicron BA.1 clinical isolate at 1 x 10^4 PFU. Mice were treated BID starting at 12 hpi with vehicle and 30 mg/kg GS-5245. n = 10 mice per group. **(B)** BA.1 lung infectious viral titers were measured at 2, 3, and 4 dpi in mice treated with vehicle or GS-5245 and 30 mg/kg at 12 hpi. Asterisks denote significant p values from a Kruskal-Wallis test after a Dunn's multiple comparisons test where * $p \leq 0.05$, ** $p \leq 0.01$, *** $p \leq 0.001$, **** $p \leq 0.0001$. **(C)** Macroscopic lung discoloration at 4 dpi is shown for therapeutically treated mice compared to vehicle **(D)** Microscopic ATS acute lung injury pathology scoring at 4 dpi is shown for vehicle vs. GS-5245-treated mice. **(E)** Microscopic DAD acute lung injury pathology scoring at 4 dpi is shown for vehicle vs. GS-5245-treated mice. For all panels, each symbol represents data for one mouse and the line is at the mean. For (C to E), Asterisks denote significant p values from a Mann-Whitney test where * $p \leq 0.05$, **** $p \leq 0.0001$. This study was performed once.

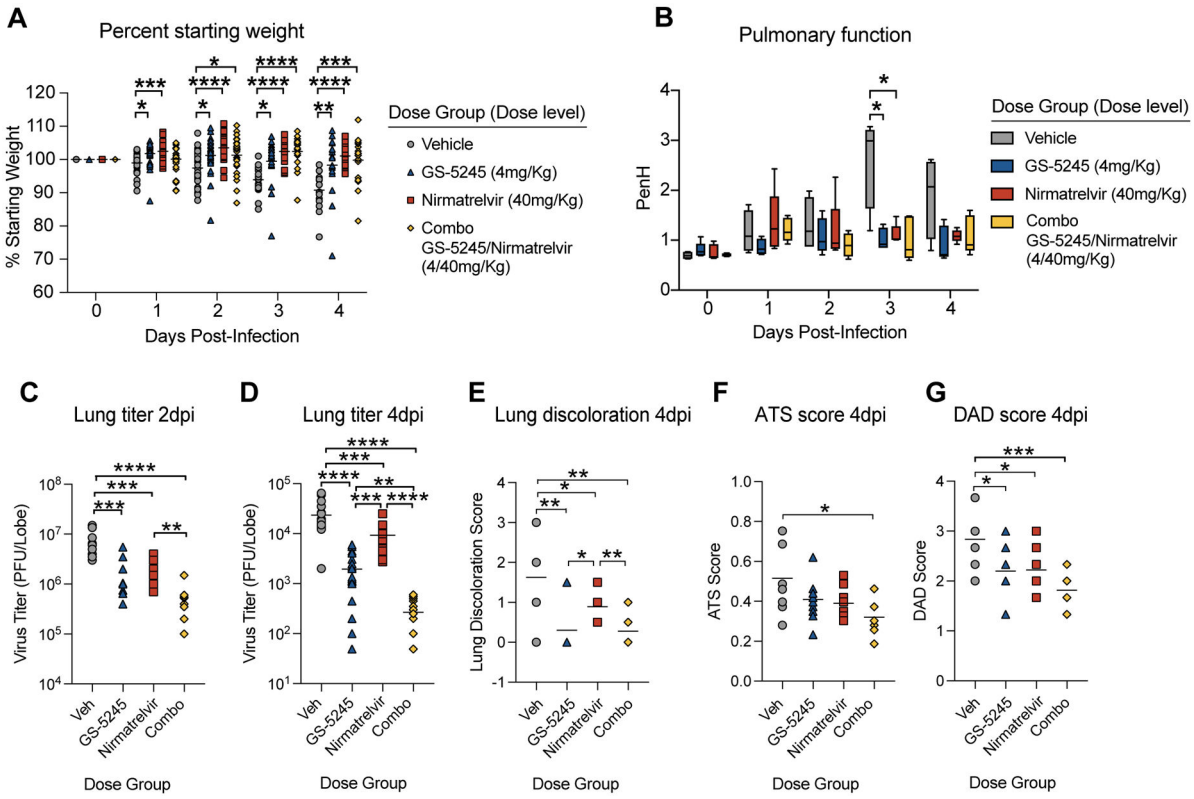

Fig. 7. Combination GS-5245 and nirmatrelvir therapy diminishes SARS-CoV-2 pathogenesis in mice.

(A) Shown is the percent change compared with starting weight in 10-week-old female BALB/c mice infected with SARS-CoV-2 MA10 at 1 x 10^4 PFU. Mice were treated BID starting at 12 hpi with vehicle (n = 28), 4 mg/kg GS-5245 (n = 30), 40 mg/kg nirmatrelvir (n = 29), or a combination of 4mg/kg GS-5245 and 40 mg/kg nirmatrelvir (n = 29). Asterisks indicate statistical significance by mixed-effects model followed by a Tukey's multiple comparisons test where * $p \leq 0.05$, *** $p \leq 0.001$, **** $p \leq 0.0001$. **(B)** Pulmonary function as measured by whole-body plethysmography in SARS-CoV-2-infected mice is shown starting at day 0 through 4 dpi. n = 4 to 5 mice per group were evaluated each time. The boxes encompass the 25th to 75th percentile, whereas the whiskers represent the range. **(C)** SARS-CoV-2 lung titers measured at 2dpi. n = 10 per group. **(D)** SARS-CoV-2 lung titers measured at 4dpi. Vehicle n = 18, GS-5245 n = 20, nirmatrelvir n = 19, combination n = 19. **(E)** Macroscopic lung discoloration at measured at 4 dpi in mice. Vehicle n = 8, GS-5245 n = 10, nirmatrelvir n = 9, combination n = 9. **(F)** Microscopic ATS acute lung injury score and (G) Diffuse alveolar damage (DAD) score measured at 4dpi. Vehicle n = 8, GS-5245 n = 10, nirmatrelvir n = 9, combination n = 9. For (A), (C), (D), (E), (F) and (G), each symbol represents data for one mouse and the line is at the mean. For (B), (C), (D), (E), (F) and (G), asterisks indicate statistical significance by Mann-Whitney test where * $p \leq 0.05$, ** $p \leq 0.01$, *** $p \leq 0.001$, **** $p \leq 0.0001$. For (A) and (D), data shown are combined from two independent experiments. All other panels are from a single study.